Near-Ultraviolet-Sensitive Graphene/Porous Silicon Photodetectors

Jungkil Kim, Soong Sin Joo, Kyeong Won Lee, Ju Hwan Kim, Dong Hee Shin, Sung Kim, and Suk-Ho Choi*

Department of Applied Physics, College of Applied Science, Kyung Hee University, Yongin 446-701, Korea

Ⓢ *Supporting Information*

ABSTRACT: Porous silicon (PSi) is recognized as an attractive building block for photonic devices because of its novel properties including high ratio of surface to volume and high light absorption. We first report near-ultraviolet (UV)-sensitive graphene/PSi photodetectors (PDs) fabricated by utilizing graphene and PSi as a carrier collector and a photoexcitation layer, respectively. Thanks to high light absorption and enlarged energy-band gap of PSi, the responsivity (R_i) and quantum efficiency (QE) of the PDs are markedly enhanced in the near-UV range. The performances of PDs are systemically studied for various porosities of PSi, controlled by varying the electroless-deposition time (t_d) of Ag nanoparticles for the use of Si etching. Largest gain is obtained at $t_d = 3$ s, consistent with the maximal enhancement of R_i and QE in the near UV range, which originates from the well-defined interface at the graphene/PSi junction, as proved by atomic- and electrostatic-force microscopies. Optimized response speed is ~10 times faster compared to graphene/single-crystalline Si PDs. These and other unique PD characteristics prove to be governed by typical Schottky diode-like transport of charge carriers at the graphene/PSi junctions, based on bias-dependent variations of the band profiles, resulting in novel dark- and photocurrent behaviors.

KEYWORDS: graphene, porous Si, Schottky diode, photodetectors, near-ultraviolet
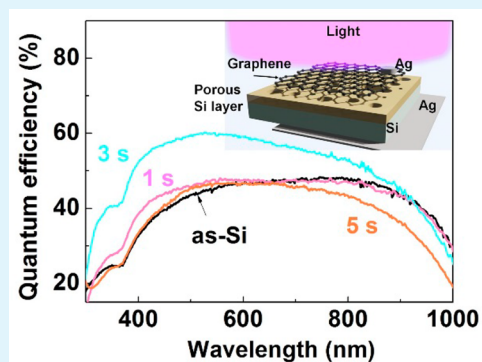
1. INTRODUCTION

Nanostructured silicon such as porous silicon (PSi) has been utilized as an attractive building block for photonic devices such as solar cells and photodetectors (PDs) due to its high light absorption, high photoconductive response, high optical gain, and high ratio of surface to volume.[1−4] Si nanostructures under 10 nm scale is governed by quantum confinement effect (QCE), by which the band gap engineering of Si can be performed, even though its effect is known to be considerably influenced by the surface defects.[5,6] Controlling the band gap energy of Si by the formation of Si nanostructures makes the light absorption/emission tunable in a particular wavelength range, and therefore, near-ultraviolet (UV)-sensitive photonic devices can be realized by employing Si nanostructures.

Applications of graphene in flexible and transparent electrodes are potentially available because graphene has outstanding physicochemical properties such as transparency over 97%, strong mechanical strength/flexibility, high electrical transportation, and excellent thermal conductivity.[7,8] A lot of efforts have been made to develop graphene-based electrodes as a promising candidate for replacing Indium Tin Oxide (ITO).[9] Some previous studies have shown successful improvements of electrical and optical properties of graphene for using graphene as transparent electrodes in photonic devices.[10] In this regard, the formation of graphene/nanostructured-Si heterostructures is very promising for their applications in photonic devices such as photodetectors (PDs). Previously, it has been reported that several Si-based heterostructures such as grapehene/bulk Si[11,12]

and graphene/metal-decorated Si nanowires (Si NWs)[13] can be useful for PDs with high photoresponsivity. However, the Si-NW-heterostructure PDs are just bulk-Si-PD-like, showing near-IR sensitivity and hundreds-of-microseconds response time,[6,13] despite small diameter of the Si NWs down to ~20 nm, and the response time of the bulk-Si-heterostructure PDs is just on the order of milliseconds.[12,13]

Here, we first demonstrate that the graphene/PSi-heterostructure PDs in a typical Schottky diode configuration, where PSi acts as a photoexcitation layer, exhibit relatively efficient and fast photoresponse in the near-UV wavelength range under low bias. The chemical-vapor-deposition-grown (CVD) graphene in large area is utilized as a carrier collector in these PDs. The performance of the PDs is discussed based on their systematical structural, electrical, and optical characterizations.

2. RESULTS AND DISCUSSION

2.1. Fabrication. Figure 1a shows a schematic diagram of graphene/PSi/n-Si PD. The PSi was prepared by conventional metal assisted chemical etching (MacEtch) of lightly doped n-type Si substrate.[14,15] The details of the fabrication processes are described in the Experimental Section. Scanning electron microscopy (SEM) images in Figure 1c−e show high-pore-density PSi surfaces for various times of electroless deposition
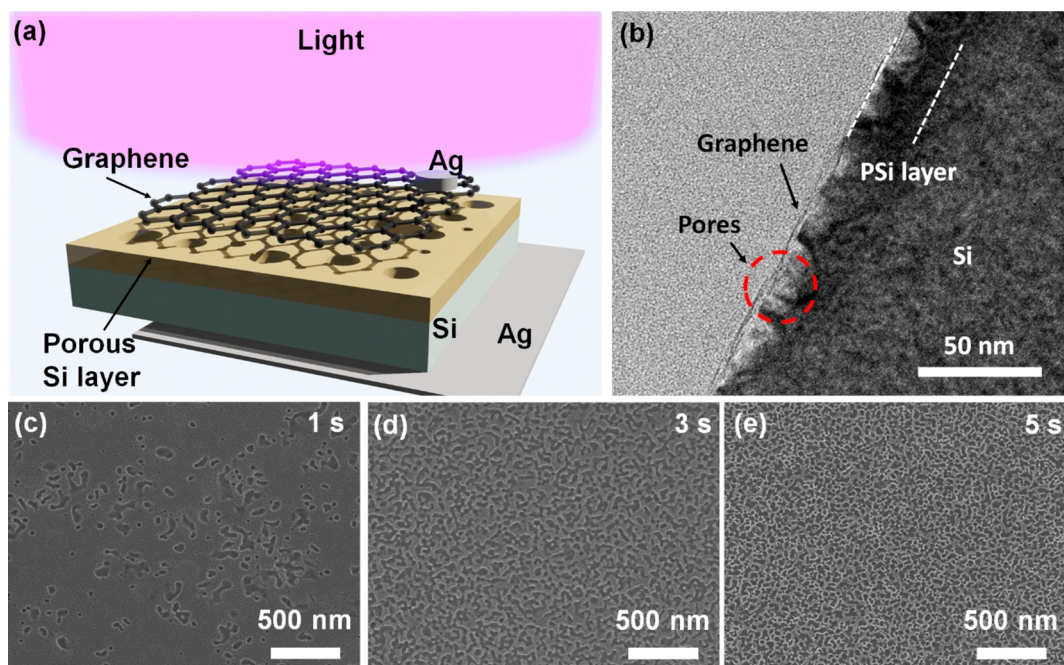
Figure 1. (a) Schematic diagram of graphene/PSi/n-Si photodetector with silver top and bottom electrodes under light illumination. (b) Cross-sectional TEM image of graphene/PSi junction. (c−e) SEM images of PSi at t_d = 1, 3, and 5 s, respectively.

(t_d) of Ag nanoparticles (NPs). The pore depth was estimated to be ∼20 nm by SEM (Figure S1). Photoluminescence (PL) and Raman spectra were measured for the four samples including a bulk Si substrate to check whether the porosity is well controlled or not. As t_d increases, the PL increases and the Raman peak is blue-shifted (see Figure S2 in the Supporting Information), consistent with the previous reports.[16,17] The pore densities of PSi are estimated to be ∼46.5, 60.3, and 79.3% for t_d = 1, 3, and 5 s, respectively, by a computational calculation method using color-threshold images (see Figure S3 in the Supporting Information). The band gap energies were estimated via Tauc plot[18] by using the absorption coefficients measured by ellipsometry. The band gap energy of PSi is enhanced with increasing t_d from 1 to 3 s, and is much larger than that of Si wafer (see Figure S4 in the Supporting Information), but the fitted curve is not linear at t_d = 5 s, indicating amorphous Si-like feature.

CVD-grown graphene of 0.5 × 0.5 cm^2 area was transferred on Si wafer as well as on PSi substrates. A transmission electron microscopy (TEM) image in Figure 1b demonstrates good transfer of graphene on PSi that consists of extremely sharp Si nanostructures under 10 nm scale for t_d = 3 s. A SEM image also shows clear separation between graphene-covered/bare PSi regions (see Figure S5a in the Supporting Information). A lower-magnification SEM image for the full size of the sample confirms well transfer of graphene without any structural alterations on large-area PSi (see Figure S5b in the Supporting Information). Ag thin films of 1 mm diameter and 1 μm thickness were deposited on the top of graphene and the bottom of Si substrate as the top and down electrodes of graphene/Si wafer and graphene/PSi with t_d = 1, 3, and 5 s to complete the device structures, named as "as-Si, 1, 3, and 5 s" PDs, respectively.

2.2. Dark and Photo $I-V$ Characteristics. Figure 2a−c illustrate energy band diagrams of the graphene/PSi/n-Si junction with illumination under no, forward, and reverse biases, respectively (see Figure S6 in the Supporting
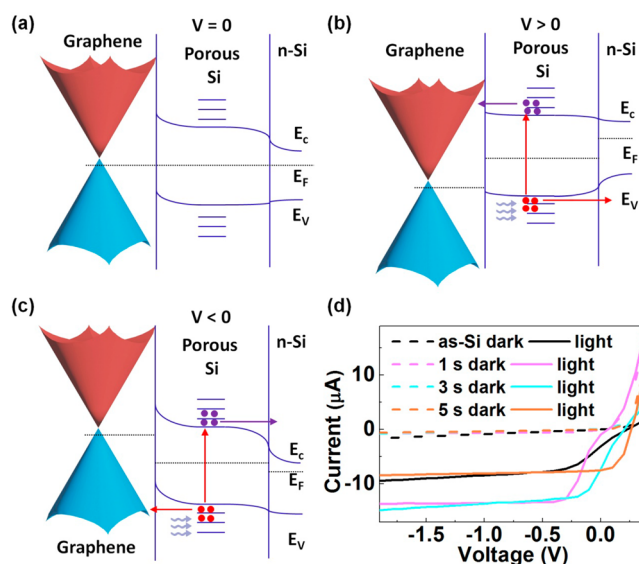

Figure 2. Band diagrams of graphene/PSi/n-Si PDs with illumination under (a) no, (b) forward, and (c) reverse biases. (d) Dark and photo $I-V$ curves of as-Si, 1, 3, and 5 s PDs under reverse bias. The excitation wavelength is 400 nm.

Information for the band diagrams without illumination). We assume that the Fermi level of PSi is located almost at the center of the band gap, regardless of the doping level of the starting Si wafer, based on the fact that the pores are formed dominantly at defect and dopant sites of Si in MacEtch,[17] thereby considerably reducing the doping concentration of Si. The band gap energy of PSi is widened compared to that of solid Si wafer, due to the QCE of Si nanostructures, and surface defects of PSi can generate additional accessible states trapping carriers.[19,20] Figure 2d shows reverse-biased $I-V$ curves of the four devices under dark and illumination (see Figure S7 in the Supporting Information for the full-range $I-V$ curves). The
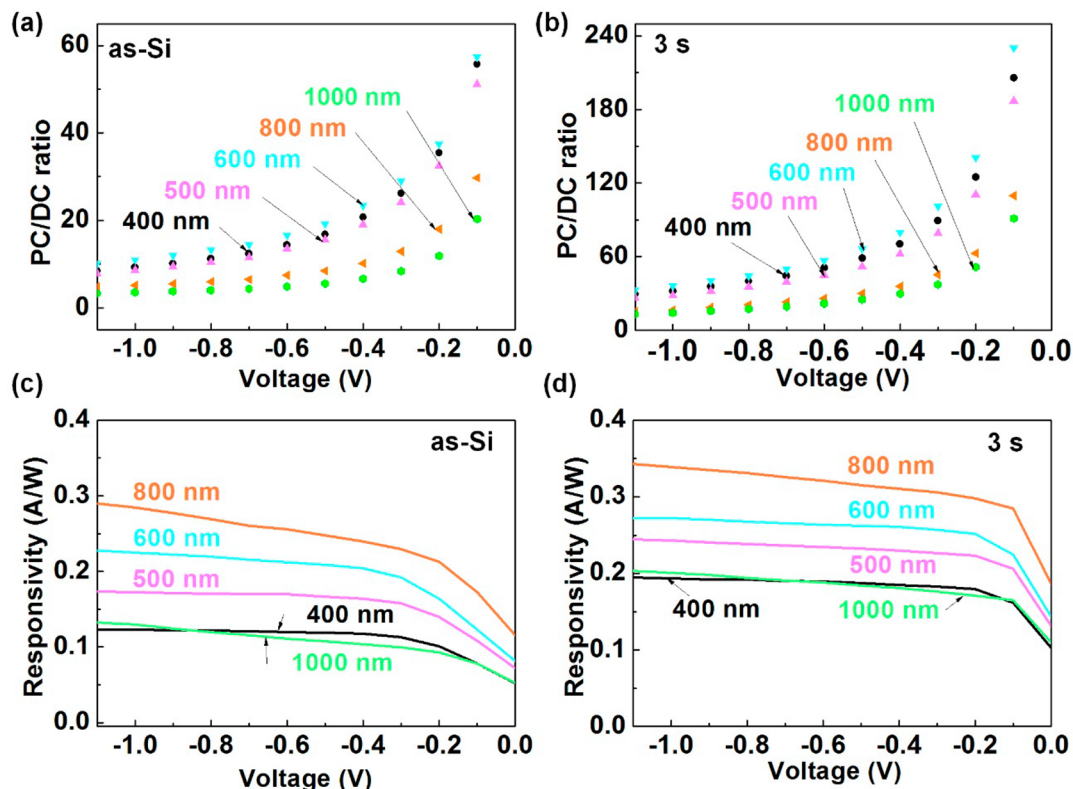
Figure 3. Bias-dependent responsivities of (a) as-Si and (b) 3 s PDs under illumination at various wavelengths from 400 to 1000 nm. Bias-dependent PC to DC ratios of (c) as-Si and (d) 3 s PDs under illumination at various wavelengths from 400 to 1000 nm.

illumination was done at a wavelength of 400 nm. All the I−V curves show typical Schottky diode-like behaviors. Under forward bias ($V > 0$), both potential barriers at the PSi/n-Si and grapene/PSi interfaces are lowered, as shown in Figure 2b, resulting in a large flow of majority carriers (electrons) from n-Si to graphene, thereby enhancing the dark current (DC). In contrast, under reverse bias ($V < 0$), almost no supply of majority carriers occurs from graphene due to the large potential barrier at the graphene/PSi junction, resulting in negligible DC, consistent with the dark I−V curves in Figure 2(d) (and Figure S7 in the Supporting Information). By the fitting of the I−V curves based on the well-known Schottky-diode equation,[21] the barrier height and the ideality factor are estimated to be 0.9−1 eV and 3.5−7, respectively. The ideality factors are a bit larger than those previously reported for graphene/Si-NW PDs.[22]

When the device is illuminated, absorption of photons in PSi produces electron−hole pairs. Under low forward bias, a negligible change in the total current between before and after light illumination, as shown in Figure 2(d), thereby making photocurrent (PC) invisible because the total current is given by (DC+PC). Even at higher forward bias, the total current is at most a factor of 2 times larger than DC (see Figure S7 in the Supporting Information), indicating little PC. Because no barrier for electrons exists between PSi and n-Si under reverse bias, as shown in Figure 2c, a large PC almost invariant with increasing reverse bias voltage is observed, as shown in Figure 2d. These results suggest that at low voltages the PDs are more photosensitive under reverse bias than under forward bias, irrespective of t_d. So, the photoresponse was in detail analyzed for the reverse-biased PDs in this work.

2.3. Photosensitivity and Quantum Efficiency. The photoresponse of PDs strongly depends on the photon wavelength. The ratios of PC to DC or the on/off ratios of as-Si, 3 s, and 5 s PDs are proportional to bias voltage, and reaches maxima at −0.1 V for various wavelengths (λ), as shown in Figure 3a, b (and Figure S8 in the Supporting Information). In contrast, the on/off ratio of 1 s PD shows a weak dependence on bias and its magnitude is relatively low (Figure S8). The PC to DC ratios of 3 and 5 s PDs are around 2−4 times larger than that of as-Si PD. Panels c and d in Figure 3 show responsivities (the electrical current response to the incident optical power, R_i) of as-Si and 3 s PDs measured as a function of bias voltage for various λ (see Figure S8 in the Supporting Information for 1 and 5 s PDs). These results suggest that the R_i strongly depends on the photon wavelength and t_d of PSi. The 3 s PD shows higher R_i than the as-Si PD over the wide range of λ. Especially, the R_i near UV range (400 and 500 nm) increases markedly by inserting the PSi layer in the device. The performances of 1 and 5 s PDs are below that of 3 s PD (see Figure S8 in the Supporting Information), indicating that 3 s seems to be the optimum deposition time. As shown in the spectral R_i of 3 s PD (see Figure S9 in the Supporting Information), there are almost no variations in R_i from −0.2 to −1.0 V. The R_i in the near UV range (400−500 nm) reaches ∼0.2 A W$^{1−}$, whist at ∼950 nm it is enhanced to ∼0.35 A W$^{1−}$. In addition, the photovoltage responsivity of 3 s device is estimated to show a linearly increasing behavior by decreasing incident light power with a highest value of ∼1 × 10^5 V/W at ∼1 μW (see Figure S10 in the Supporting Information), similar to that of the previous report.[11]

Figure 4a shows normalized spectral R_i of all PDs, indicating strong dependence of the photoresponse on t_d. By inserting the
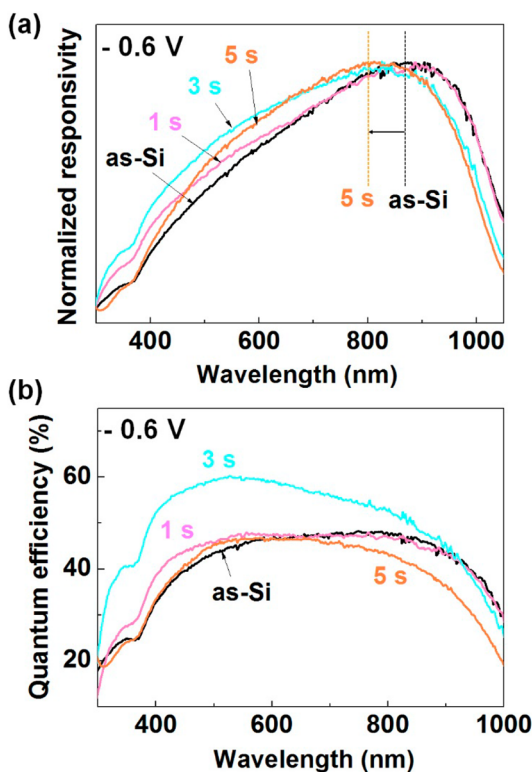
Figure 4. (a) Normalized spectral responsivities and (b) quantum efficiencies of as-Si, 1, 3, and 5 s PDs.

PSi layer in the PDs (1, 3, and 5 s), the peak wavelength of R_i is blue-shifted and the R_i in the near-UV range is enhanced. The 3

s PD shows a largest enhancement in R_i. The quantum efficiency (QE) can be calculated by normalizing the number of photogenerated carriers by the number of absorbed photons for any given λ. The QEs of all PSi PDs are enhanced in the near UV range with the change being markedly high in 3 s PD, as shown in Figure 4(b). The peak QE of 3 s PD is as high as 50−60% at around 400−500 nm. In the NIR range, there is almost no big change in QEs of 1 and 3 s PDs, but a considerable decrease is observed in 5 s PD. The behaviors of the spectral QE are consistent with those of the spectral R_i, as shown in Figure 4a. These results are comparable to the performances of single-layer graphene/Si wafer PDs, showing about 60% and 0.3 A/W in QE and R_i at 600 nm, respectively.[11]

The near-UV-sensitive photoresponse of PSi PDs can be understood by the high light absorption[23] and the enlarged energy band gap of PSi. The light absorption of PSi PDs (1, 3, and 5 s) is much larger than that of as-Si PD in the UV range with the absorption being proportional to the porosity (see Figure S11 in the Supporting Information). As shown above, the Si nanostructures in PSi increase the band gap of PSi compared to bulk Si. The origin of the size-dependent variations of the energy band gap is still a contentious issue in the field of Si-related nanostructures, but it is widely accepted that there are two dominant factors for enhancing the absorption of PSi in the near UV range; one is the QCE and the other is defect states on the surface.[24−26] However, despite the largest light absorption of 5 s PD, it does not show highest PD performance, as shown in Figures 3 and 4, possibly resulting from the amorphous Si-like feature of 5 s PSi layer, as shown via the Tauc plot, which may strongly influence the PD performance. Therefore, we doubt whether the t_d-dependent differences in the PD properties originate from the QCE or not.
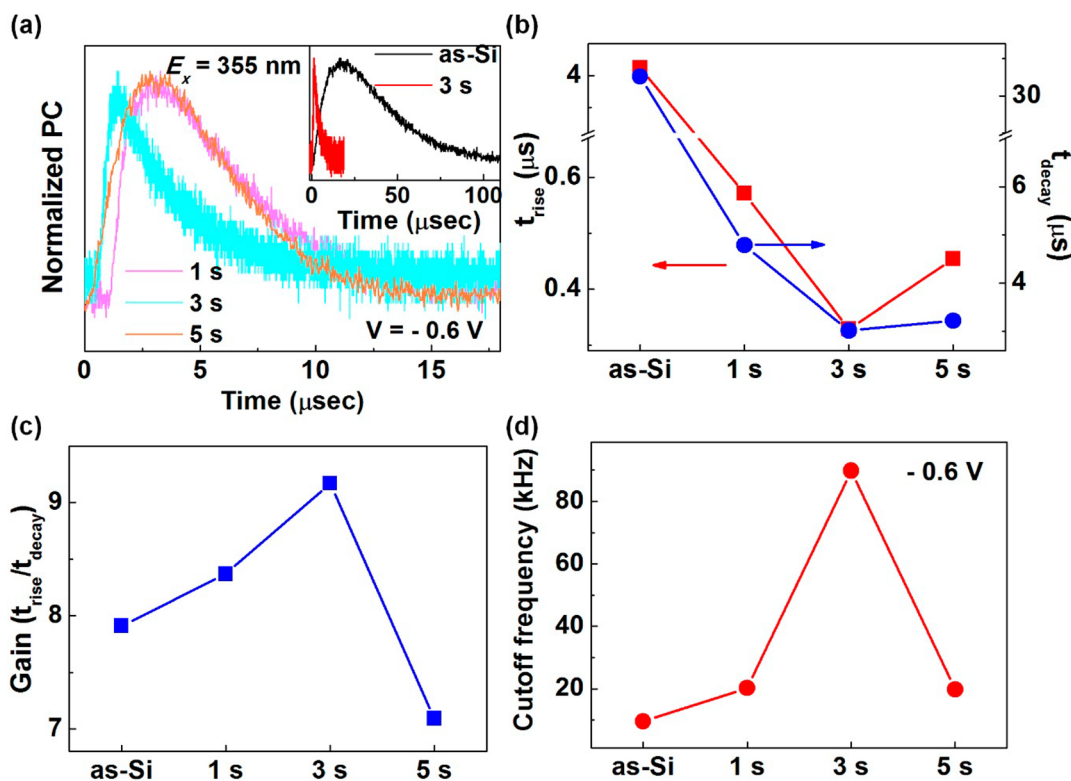

Figure 5. (a) Normalized transient PCs of as-Si, 1, 3, and 5 s PDs at a reverse bias of −0.6 V under 355 nm laser illumination. The transient PC of as-Si PD is compared with that of 3 s PD in the inset. (b) Rise/decay times, (c) gain, and (d) cutoff frequency of as-Si, 1, 3, and 5 s PDs.
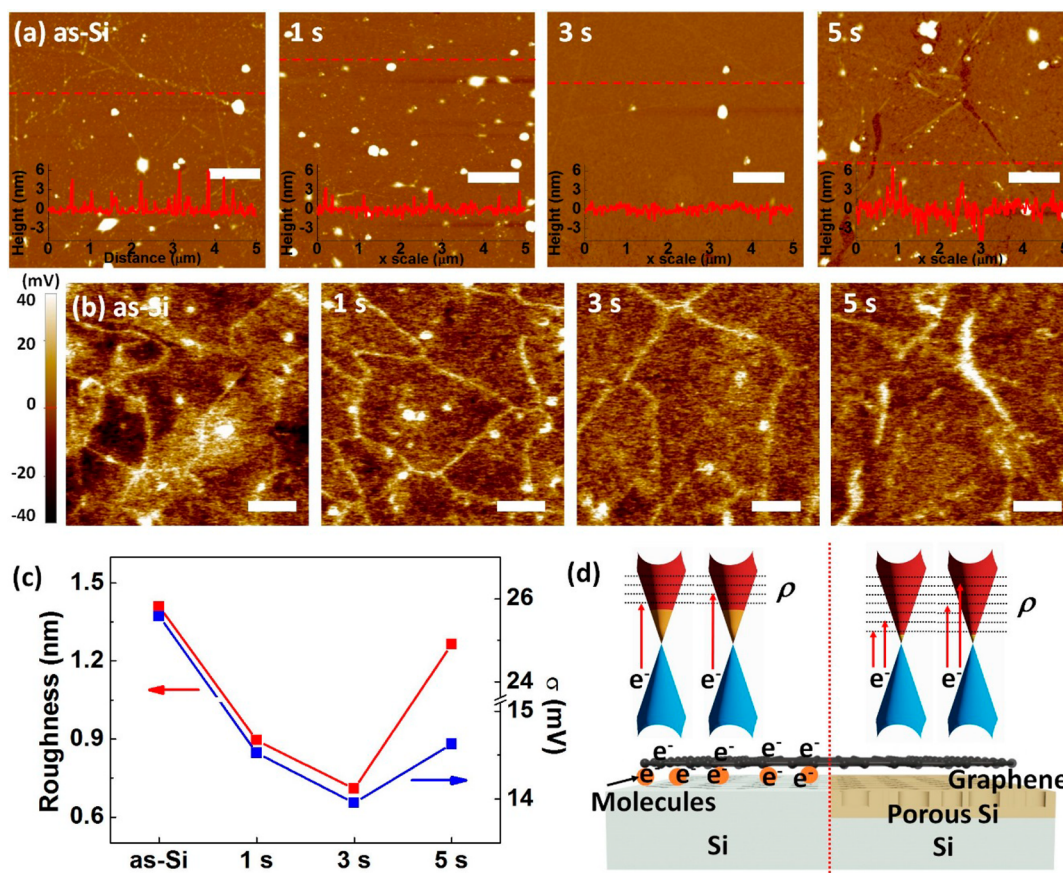
20883

dx.doi.org/10.1021/am5053812 | ACS Appl. Mater. Interfaces 2014, 6, 20880−20886

Figure 6. (a) AFM and (b) EFM images of as-Si, 1, 3, and 5 s PDs, respectively. AFM height profiles are indicated in the inset of AFM images. Here, scale bars indicate 1 μm. (c) Roughness and relative potential deviation (σ) of as-Si, 1, 3, and 5 s PDs. (d) Schematic illustrations showing different available number of final states (ρ) at the graphene/Si and graphene/PSi interfaces.

To clarify this issue, the effect of the morphological disorder will be further discussed based on the atomic force microscopy (AFM) and electrostatic force microscopy (EFM) data in later section.

2.4. Time Response. Figure 5a shows normalized transient PCs at a bias of −0.6 V under pulsed-laser excitation at 355 nm to probe charge-transfer dynamics in the near-UV range. The turn-on transient response is characterized by a relatively fast increase in the PC during t_{rise} (~several hundreds of ns), followed by a relatively slow decay with a characteristic time t_{decay} of several microseconds to a steady-state value. The fast increase is attributed to carriers generated in the region of PSi and swept out as a drift current proportional to the built-in electric field. The rise time t_{rise} is the time required for generation and transport of carriers in the graphene/PSi/n-Si structures. PSi PDs (1, 3, and 5 s) show faster rise and decay of PC than as-Si PD, as shown in Figure 5a and the inset. The rise and decay of 3 s PD are even faster, as summarized in Figure 5b, than those of the other two PSi PDs. Especially, the decay time of 3 s PD (~3 μs) is extremely short compared to the ones previously reported in graphene/Si heterostructures[11−13] (~ms). Internal gain of PDs can be estimated by the ratio of t_{decay} to t_{rise}. Largest gain is obtained for 3 s PD, consistent with highest enhancement of R_i and QE in the near UV range, as shown in Figures 5c and 4a, b. The lifetime is closely related with the frequency response of PDs.[27] The frequency response is usually evaluated by the cutoff frequency, the frequency at which the power is reduced by one-half. The

cutoff frequency is also largest as the gain for 3 s PD, as shown in Figure 5d (see Figure S12 in the Supporting Information). The PC response to periodic switches of light with intervals of 10 s is very regular (see Figure S13 in the Supporting Information). The rising and decay slops during the on/off switches are almost constant in the scale of s due to the fast response of PDs.

As similar graphene/semiconductor hybrids, graphene/ZnO/graphene PDs showed ordinary photosensitiviy and long response time of 0.5−70 s in the UV range.[21] Graphene/ZnO-NW-diode PDs responded very slowly to the UV light in the range of several ms.[28] As another approach, graphene/GaN-NW devices showed photoresponsivity of about 20 A/W under a UV light at 357 nm.[29] In contrast, the graphene/PSi PDs are not operated only in the near-UV range but also in the VIR range with relatively fast response speed.

2.5. Morphological Effects. The largest gain of 3 s PD can be understood based on the AFM and EFM results. The variation of the roughness given by the AFM images and height profiles in Figure 6a is summarized in Figure 6c. The AFM image of as-Si PD show a number of small bumps on the surface, possibly resulting from the residual molecules between graphene and underneath substrate, which gives rise to the poor contact at the interface.[30,31] Such small bumps are almost not seen on the surface of 3 s PD. The large roughness of as-Si PD could originate from the flat and hydrophobic surface of Si substrate.[30] On the other hands, the air gap of PSi can eliminate the residual molecules easily from the graphene/PSi interface,

which lead to the decrease of the roughness of PSi. In contrast, if the porosity is too high (t_d = 5 s), graphene can barely stand on air-gap or sharp-Si bridges between many vacant pores, possibly thereby making the graphene sheet torn, as shown in Figure 6a, resulting in the increase of the roughness of 5 s PD.

The EFM has been recognized as a reliable tool to analyze the work function on the device surfaces,[32,33] and well employed to explain the effect of doping on carrier lifetimes in graphene.[34] The EFM images in Figure 6(b) give the relative electrostatic potential deviations (σ) on the PD surfaces, as summarized in Figure 6(c). The variation of σ is very similar to that of the roughness. The residual molecules between graphene and Si (or PSi) substrate might trap electrons,[35,36] resulting in the formation of electrostatic potential on the PD surfaces. The work function is expressed as $W = -e\emptyset - E_f$, where $-e$ is the charge of an electron, E_f is the Fermi level, and $\emptyset$ is the electrostatic potential. As the electrostatic potential of the PD surfaces decreases, more final states are unoccupied, indicating the increase of the available number of final states per unit energy, ρ (Figure 6d). According to the Fermi golden rule, ρ is closely related with transition rate (T), as expressed in the formula: $T_{i \to f} = 2\pi/\hbar|\langle f|H'|i\rangle|^2\rho$, where $\int|H'|i$ is the matrix element of the perturbation H' between the final and initial states. As a result, T is proportional to ρ. T is inversely proportional to lifetime based on the spontaneous emission theory.[37] So, it can be easily expected that t_{decay} is proportional to σ, consistent with Figures 5b and 6c. This also explains why the gain is largest in 3 s PD, as shown in Figure 5c.

3. CONCLUSION

Near-UV-sensitive graphene/PSi PDs were successfully fabricated by employing graphene and PSi as a carrier collector and a photoexcitation layer, respectively. The control of the porosity by varying t_d was confirmed by SEM, PL, and Raman spectroscopy. The R_i and QE of the PDs remarkably enhanced in the near-UV range were attributed to the high light absorption and enlarged energy band gap of PSi. The largest gain was obtained at t_d = 3 s, consistent with the largest enhancement of R_i and QE in the near UV range, which originated from the well-defined interface at the graphene/PSi junction of 3 s PD, as proved by AFM and EFM. The unique PD characteristics were shown to be governed by typical Schottky diode-like transport of charge carriers at the graphene/PSi junctions, based on bias-dependent variations of the band profiles. The PSi PDs, especially at t_d = 3 s, showed extremely high speed of photoresponse, as short as ~3 μs in t_{decay}, compared to the as-Si PD. The performances of graphene/PSi PDs can be further enhanced by optimizing the electrode material/structure and the pore depth. These results suggest that PSi can be utilized as a new building block for near-UV-sensitive photonic devices including PDs and solar cells.

■ EXPERIMENTAL SECTION

For the fabrication of PSi, Ag NPs as MacEtch catalyst were first deposited on the Si surface in the $AgNO_3$ solutionl. Second, MacEtch of Si was performed in the HF and H_2O_2 mixture solution. During this process, the Si part attached with Ag NPs was selectively etched down, thereby generating pores on the Si surface. The porosity of Si was controlled by varying t_d of Ag NPs from 1 to 5 s in the $AgNO_3$ (5 mM) and HF (5 M) mixed deposition solution. Immediately, each Si substrate with Ag NPs was immersed in a mixed etchant of HF, H_2O_2, and H_2O ([HF]:[H_2O_2]:[H_2O] = [2.4]:[0.1]:[50.0]) for 5 s at the room temperature (RT). Finally, the remanent Ag NPs were removed in HNO_3 for a minute.

Graphene layers were grown on 70 μm thick Cu foils (Wacopa, 99.8 purity) in a graphite-heater-based CVD quartz tube furnace at a growth temperature of 1000 °C with 10 sccm H_2 and 20 sccm CH_4 flowing at a pressure of 3 Torr. The graphene/Cu stack was spin-coated with poly(methyl methacrylate) (PMMA), and the Cu was then etched in 1 M ammonium persulfate for 10 h. The graphene/PMMA stack was then placed in deionized water before transferring to the PSi/n$^+$-type Si wafers and blow-dried with dry N_2. The PMMA/graphene/PSi/Si stack was then heated on a hot plate in air at 180 °C for 2 h to cure the PMMA. This heating temperature was selected because it is slightly higher than the glass transition temperature of PMMA (<165 °C), which allows the PMMA to reflow when it is annealed. This process has been found to transfer graphene layers more uniformly with their cracking minimized. After the samples were cooled to RT, the PMMA was stripped by soaking them in acetone for 1 h at RT.

Raman spectra of graphene films were measured by using a 532 nm (~2.33 eV) laser line for excitation. Raman spectra of transferred graphene exhibited two intense features, G and 2D peaks at ~1590 and ~2685 cm^{-1}, respectively. A relatively small Raman feature at ~1350 cm^{-1} was identified with a disorder-induced band or D band. PL spectra were measured at RT using the 325 nm line of a He−Cd laser as the excitation source. Emitted light was collected by a lens and analyzed using a grating monochromator and a GaAs photomultiplier tube. SEM images were taken at various magnifications by using field-emission scanning electron microscope (Leo Supra 55, Carl Zeiss) at the acceleration voltage of 10 kV. TEM samples were prepared by using Dual Beam FIB System (Nova 200, FEI). TEM images were taken by using FE-TEM (JEM-2100F HR, JEOL) at the acceleration voltage of 200 kV. The AFM and EFM images were taken by using AFM systems (XE-100, Park Systems). The bias applied to the EFM tip was 1.0 V for all devices.

$I-V$ measurements to characterize the electrical behaviors were carried out using a Keithley 2400 source meter controlled by a LabView program. During the measurements, the PDs were mounted in a dark, electrically shielded, and optically sealed chamber on the optical table to reduce vibrational noise. The light source with specific wavelengths is generated by using a 450 W xenon lamp and a 0.25-m grating monochromator. The incident light intensity was monitored by a motorized variable wheel attenuator and a Newport calibrated UV enhanced silicon photodiode. The power density of the incident light on the sample surface was about 1−320 W/cm^2 depending on the wavelength in the range of 300−1100 nm. Transient PC studies were conducted using laser pulses from the Nd:YAG laser (532 nm wavelength, 20 ps duration and 20 Hz repetition rate, generated by a Continuum Leopard-D20 Nd:YAG laser), which were focused onto the PD devices with a spot size of ~5 × 5 mm^2. A laser power meter (Laser probe, Rj-760) was used to measure the average power of the laser pulses. The transient PCs were monitored with the 50 ohm terminated, 500 MHz bandwidth digital oscilloscope (Tektronix DPO 4054). For frequency dependence of the PC, the PDs were illuminated by a Thorlabs 50 μW, 530 nm light emitting diode (LED) array with an Instek SFG 830 30 MHz function generator used to supply a constant or modulated bias to the LEDs. The PC response was measured with a SR 530 lock-in amplifier coupled to a current preamplifier (Stanford Research SR 570) in the frequency range of 1 Hz to 100 kHz.

■ ASSOCIATED CONTENT

ⓢ Supporting Information

Figure S1, cross-sectional SEM image; Figure S2, PL and Raman spectra; Figure S3, threshold SEM images; Figure S4, Tauc plots; Figure S5, plan-view SEM images; Figure S6, band diagram of graphene/PSi/n-Si PDs without illumination; Figure S7, full-range dark and photo $I-V$ curves; Figure S8, bias-dependent PC to DC ratios and responsivities; Figure S9, spectral responsivities; Figure S10, photovoltage responsivity of 3 s device; Figure S11, absorption spectra; Figure S12,

frequency-dependent PC response; Figure S13, PC response to periodic switches of light. This material is available free of charge via the Internet at http://pubs.acs.org.

■ AUTHOR INFORMATION

Corresponding Author
*E-mail: sukho@khu.ac.kr. Fax: +82-31-204-8122.
Notes
The authors declare no competing financial interest.

■ ACKNOWLEDGMENTS

■ REFERENCES

(1) Law, M.; Greene, L. E.; Johnson, J. C.; Saykally, R.; Yang, P. D. Nanowire Dye-Sensitized Solar Cells. *Nat. Mater.* **2005**, *4*, 455−459.

(2) Avouris, P.; Freitag, M.; Perebeinos, V. Carbon-Nanotube Photonics and Optoelectronics. *Nat. Photonics* **2008**, *2*, 341−350.

(3) Yan, R. X.; Gargas, D.; Yang, P. D. Nanowire Photonics. *Nat. Photonics* **2009**, *3*, 569−576.

(4) Spurgeon, J. M.; Boettcher, S. W.; Kelzenberg, M. D.; Brunschwig, B. S.; Atwater, H. A.; Lewis, N. S. Flexible, Polymer-Supported, Si Wire Array Photoelectrodes. *Adv. Mater.* **2010**, *22*, 3277−3281.

(5) Park, N. M.; Choi, C. J.; Seong, T. Y.; Park, S. J. Quantum Confinement in Amorphous Silicon Quantum Dots Embedded in Silicon Nitride. *Phys. Rev. Lett.* **2001**, *86*, 1355−1357.

(6) Walavalkar, S. S.; Hofmann, C. E.; Homyk, A. P.; Henry, M. D.; Atwater, H. A.; Scherer, A. Tunable Visible and Near-IR Emission from Sub-10 nm Etched Single-Crystal Si Nanopillars. *Nano Lett.* **2010**, *10*, 4423−4428.

(7) Geim, A. K.; Novoselov, K. S. The Rise of Graphene. *Nat. Mater.* **2007**, *6*, 183−191.

(8) Lee, C.; Wei, X. D.; Kysar, J. W.; Hone, J. Measurement of the Elastic Properties and Intrinsic Strength of Monolayer Graphene. *Science* **2008**, *321*, 385−388.

(9) Das, A.; Pisana, S.; Chakraborty, B.; Piscanec, S.; Saha, S. K.; Waghmare, U. V.; Novoselov, K. S.; Krishnamurthy, H. R.; Geim, A. K.; Ferrari, A. C.; Sood, A. K. Monitoring Dopants by Raman Scattering in an Electrochemically Top-Gated Graphene Transistor. *Nat. Nanotechnol.* **2008**, *3*, 210−215.

(10) Shin, D. H.; Lee, C. W.; Lee, J. S.; Kim, J. H.; Kim, S.; Choi, S.-H. Enhancement of the Effectiveness of Graphene as a Transparent Conductive Electrode by AgNO₃ Doping. *Nanotechnology* **2014**, *25*, 125701.

(11) An, X. H.; Liu, F. Z.; Jung, Y. J.; Kar, S. Tunable Graphene-Silicon Heterojunctions for Ultrasensitive Photodetection. *Nano Lett.* **2013**, *13*, 909−916.

(12) Lv, P.; Zhang, X. J.; Zhang, X. W.; Deng, W.; Jie, J. S. High-Sensitivity and Fast-Response Graphene/Crystalline Silicon Schottky Junction-Based Near-IR Photodetectors. *IEEE Electron Device Lett.* **2013**, *34*, 1337−1339.

(13) Luo, L. B.; Zeng, L. H.; Xie, C.; Yu, Y. Q.; Liang, F. X.; Wu, C. Y.; Wang, L.; Hu, J. G. Light Trapping and Surface Plasmon Enhanced High-Performance NIR Photodetector. *Sci. Rep.* **2014**, *4*, 3914.

(14) Li, X.; Bohn, P. W. Metal-Assisted Chemical Etching in HF/H₂O₂ Produces Porous Silicon. *Appl. Phys. Lett.* **2000**, *77*, 2572.

(15) Kim, J.; Han, H.; Kim, Y. H.; Choi, S. H.; Kim, J. C.; Lee, W. Au/Ag Bilayered Metal Mesh as a Si Etching Catalyst for Controlled Fabrication of Si Nanowires. *ACS Nano* **2011**, *5*, 3222−3229.

(16) Deb, S. K.; Wilding, M.; Somayazulu, M.; McMillan, P. F. Pressure-Induced Amorphization and an Amorphous-Amorphous Transition in Densified Porous Silicon. *Nature* **2001**, *414*, 528−530.

(17) Qu, Y. Q.; Liao, L.; Li, Y. J.; Zhang, H.; Huang, Y.; Duan, X. F. Electrically Conductive and Optically Active Porous Silicon Nanowires. *Nano Lett.* **2009**, *9*, 4539−4543.

(18) Grivickas, V.; Basmaji, P. Oprical Absorption in Porous Silicon of High Porosity. *Thin Solid Films* **1993**, *235*, 234−238.

(19) Heitmann, J.; Muller, F.; Yi, L. X.; Zacharias, M.; Kovalev, D.; Eichhorn, F. Excitons in Si Nanocrystals: Confinement and Migration Effects. *Phys. Rev. B* **2004**, *69*, 195309.

(20) Herbert, F. W.; Krishnamoorthy, A.; Van Vliet, K. J.; Yildiz, B. Quantification of Electronic Band Gap and Surface States on FeS₂(100). *Surf. Sci.* **2013**, *618*, 53−61.

(21) Fu, X. W.; Liao, Z. M.; Zhou, Y. B.; Wu, H. C.; Bie, Y. Q.; Xu, J.; Yu, D. P. Graphene/ZnO Nanowire/Graphene Vertical Structure Based Fast-Response Ultraviolet Photodetector. *Appl. Phys. Lett.* **2012**, *100*, 223114.

(22) Fan, G.; Zhu, H.; Wang, K.; Wei, J.; Li, X.; Shu, Q.; Guo, N.; Wu, D. Graphene/Silicon Nanowire Schottky Junction for Enhanced Light Harvesting. *ACS Appl. Mater. Interfaces* **2011**, *3*, 721−725.

(23) Chan, M. H.; So, S. K.; Cheah, K. W. Optical Absorption of Free-Standing Porous Silicon Films. *J. Appl. Phys.* **1996**, *79*, 3273−3275.

(24) Park, J. Y.; Song, D. E.; Kim, S. S. An Approach to Fabricating Chemical Sensors Based on ZnO Nanorod Arrays. *Nanotechnology* **2008**, *19*, 105503.

(25) Ahn, M. W.; Park, K. S.; Heo, J. H.; Kim, D. W.; Choi, K. J.; Park, J. G. On-Chip Fabrication of ZnO-Nanowire Gas Sensor with High Gas Sensitivity. *Sens. Actuators, B* **2009**, *138*, 168−173.

(26) Yuan, G. D.; Zhou, Y. B.; Guo, C. S.; Zhang, W. J.; Tang, Y. B.; Li, Y. Q.; Chen, Z. H.; He, Z. B.; Zhang, X. J.; Wang, P. F.; Bello, I.; Zhang, R. Q.; Lee, C. S.; Lee, S. T. Tunable Electrical Properties of Silicon Nanowires via Surface-Ambient Chemistry. *ACS Nano* **2010**, *4*, 3045−3052.

(27) Novak, S.; Moesle, A. Analytic Model for Gain Modulation in EDFAs. *J. Lightwave Technol.* **2002**, *20*, 975−985.

(28) Nie, B.; Hu, J. G.; Luo, L. B.; Xie, C.; Zeng, L. H.; Lv, P.; Li, F. Z.; Jie, J. S.; Feng, M.; Wu, C. Y.; Yu, Y. Q.; Yu, S. H. Monolayer Graphene Film on ZnO Nanorod Array for High-Performance Schottky Junction Ultraviolet Photodetector. *Small* **2013**, *9*, 2872−2879.

(29) Babichev, A. V.; Zhang, H.; Lavenus, P.; Julien, F. H.; Egorov, A. Y.; Lin, Y. T.; Tu, L. W.; Tchernycheva, M. GaN Nanowire Ultraviolet Photodetector with a Graphene Transparent Contact. *Appl. Phys. Lett.* **2013**, *103*, 201103.

(30) Lee, D.; Ahn, G.; Ryu, S. Two-Dimensional Water Diffusion at a Graphene-Silica Interface. *J. Am. Chem. Soc.* **2014**, *136*, 6634−6642.

(31) Meunier, M.; Quirke, N. Molecular Modeling of Electron Trapping in Polymer Insulators. *J. Chem. Phys.* **2000**, *113*, 369−376.

(32) Smith, G. X. R.; Crook, R.; Wadhawan, J. D. Measuring the Work Function of TiO₂ Nanotubes Using Illuminated Electrostatic Force Microscopy. *J. Phys. Conf. Ser.* **2013**, *471*, 012045.

(33) Panchal, V.; Pearce, R.; Yakimova, R.; Tzalenchuk, A.; Kazakova, O. Standardization of Surface Potential Measurements of Graphene Domains. *Sci. Rep.* **2013**, *3*, 2597.

(34) Mak, K. F.; da Jornada, F. H.; He, K.; Deslippe, J.; Petrone, N.; Hone, J.; Shan, J.; Louie, S. G.; Heinz, T. F. Tuning Many-Body Interaction in Graphene; The Effects of Doping on Excitons and Carrier Lifetmes. *Phys. Rev. Lett.* **2014**, *112*, 207401.

(35) Shkrob, I. A.; Schlueter, J. A. Can a Single Molecule Trap the Electron? *Chem. Phys. Lett.* **2006**, *431*, 364−369.

(36) Narevicius, E.; Moiseyev, N. Trapping of an Electron due to Molecular Vibrations. *Phys. Rev. Lett.* **2000**, *84*, 1681−1684.

(37) Loudon, R. *The Quantum Theory of Light*, 3rd ed; Oxford University Press:, New York, 2001.